Korean J. Chem. Eng., 35(1), 89-98 (2018)
DOI: 10.1007/s11814-017-0268-x

pISSN: 0256-1115
eISSN: 1975-7220

Effects of copper loading on NH_3-SCR and NO oxidation over Cu impregnated CHA zeolite

Nusnin Akter*, Xianyin Chen, John Parise**, Jorge Anibal Boscoboinik*,***, and Taejin Kim*,†**

*Materials Science and Chemical Engineering Department, Stony Brook University, Stony Brook, NY 11794, U.S.A.
**Geosciences Department, Stony Brook University, Stony Brook, NY 11794, U.S.A.
***Center for Functional Laboratory, Brookhaven National Laboratory, Upton, NY 11973, U.S.A.
(*Received 1 July 2017 • accepted 25 September 2017*)

Abstract−Cu/CHA catalysts with various Cu loadings (0.5 wt%-6.0 wt%) were synthesized via incipient wetness impregnation. The catalysts were applied to the selective catalytic reduction (SCR) of NO with NH_3 and NO oxidation reaction. XRD and N_2 adsorption-desorption data showed that CHA structure was maintained with the incorporation of Cu, while specific surface areas decreased with increasing Cu loading. At intermediate Cu loading, 4 wt%, the highest NH_3-SCR activity was observed with ~98% N_2 selectivity from 150 °C to 300 °C. Small amounts of water, 2%, slightly increased NO conversion in addition to the remarkable N_2O and NO_2 reduction at high temperature. Water effects are attributed to the improved Cu ion reducibility and mobility. NO oxidation results provided no relation between NO_2 formation and SCR activity. Physicochemical properties, NO conversion, N_2 selectivity, and activation energy data showed that impregnated samples' molecular structure and catalytic activity are comparable to the conventional ion-exchanged (IE) samples' ones.

Keywords: Chabazite Framework Zeolite, Selective Catalytic Reduction (SCR), Copper Loading, Incipient Wetness

INTRODUCTION

NO_x is the common term for mono-nitrogen oxides (NO and NO_2), which are exhausts from automobiles and stationary sources during combustion (fossil fuels in vehicles' engines or coal in electric power plants). NO_x species are toxic pollutants that cause health problems such as lung infections, respiratory allergies, bronchitis and pneumonia, as well as environmental problems such as ozone destruction, acid rain, subsequent acidification of soils and waters, eutrophication, and material corrosion [1-5]. Among various kinds of NO_x removal technologies, NO direct thermal decomposition to N_2 and O_2 is one [6]. Although NO decomposition is thermodynamically favorable, $\Delta G_f^0 = -86$ kJ/mol [5], this reaction is kinetically very difficult to achieve in the presence of oxygen due to the high activation energy of 365 kJ/mol [7]. Selective catalytic reduction (SCR) is one of the favorite technologies for NO_x removal from lean exhaust gases in automotive applications. Standard SCR is the reaction of nitric oxide (NO) with ammonia (NH_3) in the presence of oxygen to form nitrogen and water [8]:

$$4NO+4NH_3+O_2 \rightarrow 4N_2+6H_2O$$

The application of vanadia (V_2O_5) based SCR catalysts' for NO_x removal in the stationary sources (e.g., power plants) has led to the possibility and experimentation of this application in vehicles. TiO_2-supported V_2O_5, promoted with WO_3, has been commercially used in Europe for automobile applications [9]. Nevertheless, in the U.S there are concerns that vanadium oxide-based catalysts are not suited for mobile NH_3-SCR application because of their narrow operation temperature window (350-400 °C) at which a relative high conversion is achieved [10], the undesired activity in catalyzing SO_2 oxidation to SO_3, the rapid decrease in activity and selectivity at 550 °C, and the toxicity of the vanadia species, which begin to volatilize above 650 °C [11,12]. Various metal-exchanged zeolites-base metal catalysts have been also investigated for NO decomposition and SCR catalytic activity, and shown positive results in NO_x reduction, although bare zeolites did not show higher NO reduction activity [13-27]. While both Cu and Fe-zeolite catalysts are better choices than vanadia-based catalysts, it has been reported that Fe/zeolites showed lower reactivity at low temperature than Cu/zeolites [6]: the effective temperature ranges for Cu- and Fe-ZSM-5 are 250-450 °C and 350-650 °C, respectively [28].

Recently, Cu based zeolite, especially chabazite, CHA (Cu-CHA) has been selected for SCR applications because it showed exceptional hydrothermal stability in addition to the higher NO reduction activity [29]. The improved hydrothermal stability is due to small-pore structure where the largest pore has an opening of 3.8 Å with an 8-membered ring structure [30]. Chen et al. reported that catalysts with 8-membered rings display better hydrothermal stabilities than other zeolites with 10 or 12 membered rings [31]. Another important property that makes CHA type zeolite a good SCR catalyst is that CHA does not permit large molecular size hydrocarbons (diesel fuel) to enter and adsorb within the framework [32,33]. In addition to the typical aluminosilicate framework zeolites, SAPO-34 (silicoaluminophosphates) or modified SAPO-34 (e.g MeAPSO-34) has been also applied for NO_x treatment as an automotive catalyst. SAPO-34 zeotype catalysts have proven to be

†To whom correspondence should be addressed.
E-mail: taejin.kim@stonybrook.edu

uniquely effective in NH_3-SCR, in particular Cu/SAPO-34, due to its higher hydrothermal stability than Cu/SSZ-13 (most commonly used CHA structure zeolite in NH_3-SCR) [34,35]. Also, Leistner et al. [36] studied the TPR experiments and showed that Cu in Cu/SAPO-34 is more easily reduced compared to Cu/SSZ-13. This actually facilitated the redox processes and exhibited higher SCR activity at 150 °C than Cu/SSZ-13. This is important because the new SCR catalyst requirement is to work well in a wide temperature window of exhaust gas: 150-550 °C. It is indicated that the Cu-SAPO-34 catalyst had a relatively higher De-NO_x performance than the Cu-SSZ-13 catalyst across a wide range of reaction temperatures range (100-700 °C) [37].

Petitto and Delahay [38] tested SAPO-34 supported Cu (<2 wt%) catalysts with different silicon content (0.57-3.8 wt%) and Ti (0.20-1.97 wt%) for NH_3-SCR of NO reduction. They observed that ~2 wt% Ti containing SAPO-34 showed higher NO conversion compared to the SAPO-34 and SAPO-18 zeolites, although they authors show products (e.g., N_2O and NO_2) selectivity and the effect of Cu loading on NO conversion in detail. Their sample was furnished by Clariant where the Si contain is 3 wt% and the H form CHA zeolite support used in our study was very similar to this zeolite. There are several preparation techniques to put the active species at the zeolite exchange sites such as hydrothermal synthesis (HS), solid state ion exchange (SSIE), aqueous solution ion-exchanged (IE) methods reported in the literature, where IE is the most popular among them [15,30,32,39-41]. However, less attention has been given to the incipient wetness impregnation (IWI) to prepare Cu exchanged CHA framework zeolites. Table 1 shows the comparison of available Cu/CHA catalyst synthesis methods with their advantages and disadvantages.

In the present work, we prepared CHA framework zeolite supported different Cu loading (0.5-6.0 wt%) samples by IWI method to investigate NH_3-SCR and NO oxidation reaction. Specifically, we focused on the feasibility of using IWI method prepared Cu-CHA framework catalyst for catalytic activity and selectivity in the presence water. We observed that the as-prepared samples showed comparative NO reduction and high N_2 selectivity performance with and without water presence, providing that IWI method can also be applied to Cu-modified zeolite catalysts for NH_3-SCR and NO oxidation reaction.

EXPERIMENTAL

1. Catalyst Synthesis and Characterization

Commercial H form chabazite (CHA) framework (Al=21.6%, P=20.1%, Si=4.3%, Ti=1.9%) zeolite was graciously supplied by Clariant, and copper (ii) nitrate hemi (pentahydrate) (≥98%) was purchased from Sigma Aldrich. Oxygen gas (Extra Dry Grade), argon gas (UHP Grade), 2,000 ppm NO in helium, and 2,000 ppm NH_3 in helium were purchased from Praxair. 200 ppm NO_2 gas in Ar and 200 ppm N_2O gas in Ar were purchased from Global Calibration Gases LLC. A series of supported copper on CHA catalyst was synthesized using incipient wetness impregnation of aqueous copper nitrate onto CHA at room temperature. After impregnation, the samples were dried at room temperature for 12 hr and at 100 °C overnight and then calcined in flowing air (100 ml/min) at 500 °C for 4 hr with ramping rate 2 °C/min in a tubular furnace. After calcination, the samples were crushed and sieved to 450 μm in size.

Specific surface areas of the catalysts were measured by the Brunauer-Emmett-Teller (BET) method with a Quantachrome Instrument Nova 2200e surface area and pore size analyzer. Approximately 0.15 g powder sample was first evacuated at room temperature for 30 min and then heated at a rate of 2 °C/min to 225 °C under vacuum condition. The surface area was calculated from a linear BET plot acquired from analysis at liquid N_2 temperature (−196 °C) under N_2 adsorption-desorption isotherms. The pore size distributions were obtained by Barrett-Joyner-Halenda (BJH) method.

Powder X-ray diffraction (XRD) patterns were recorded on a Rigaku Miniflex diffractometer at ambient conditions using filtered Cu-K radiation (1.5406 A°) operated at 40 kV and 40 mA. Diffraction data were collected from 10 to 80° with a resolution of 0.02° (2θ). X-ray photo-electron spectroscopy (XPS) was performed

Table 1. Comparison of Cu/CHA synthesis methods

Synthesis method	Advantage	Disadvantage
Solid state ion-exchange (SSIE) [81]	- Straightforward method - Allows easily achieved Cu loading control	- Needs elevated temperature (700 °C & higher) - High temperatures partially damage the zeolites - Incomplete CuO presence after synthesis
Aqueous ion exchange (IE) [16,82]	- Most commonly used - Gives excellent catalytic performance.	- Needs several repeated cycles to achieve the desired Cu amount - 3 to 4 ion-exchanges were required to obtain high metal loading. - Surface area and pore volume dropped significantly (especially for SAPO-34) - Significant drop in zeolite crystallinity (for SAPO-34)
Impregnation method (IWI) [83]	- Catalyst with high metal loading can be obtained	- Pores are easily blocked by reactive metals
In-situ hydrothermal synthesis (HS) [67]	- Introduces the active metal into the zeolite framework during the preparation process - Simplifies the preparation	- Activity is lower than ion-exchange but higher than impregnation.

on a SPECS Phoibos 100 hemispherical analyzer using Al Kα (1,486.6 eV) X-ray source at the Center for Functional Nanomaterial at the Brookhaven National Lab. The surface charging effect during measurement was compensated by referencing the binding energy (BE) of C 1s (BE=284.6 eV) as an internal standard.

2. Catalytic Activity Measurement

Catalytic activity tests were performed using a fixed bed quartz tube reactor (3/8″ O.D and 7.6″ height) operated at atmospheric pressure. Within the reactor tube, 40 mg of a catalyst was placed in the center of the reactor. The reaction temperature of the catalyst was measured by a thermocouple (Omega, K-type) embedded within the reactor bed. The flow rate of gasses was monitored with a mass flow meter (Omega Engineering, Inc., FMA-1700A/1800A series). Catalyst was preheated at 450 °C in flowing 20% O_2/Ar (100 ml/min) for 1 hr to remove any impurities. NH_3-SCR reaction was examined in flowing a mixture of 500 ppm NO, 500 pm NH_3, 10% O_2, and Ar balance with a total gas flow rate of 200 ml/min. Catalytic activity was also examined with 2% water (H_2O) presence with other experimental conditions remaining the same (500 ppm NO, 500 pm NH_3, 10% O_2, and 2% H_2O with Ar for balance). Water vapor was generated by passing Ar gas through a heated gas-wash bottle containing deionized water. NO oxidation reaction was carried out in the absence of NH_3 and H_2O, but other experimental conditions remained the same (500 ppm NO and 10% O_2 with Ar for balance).

For catalytic activity test, the reaction temperature was studied from 450 °C to 100 °C in intervals of 50 °C. At the target reaction temperatures, a minimum waiting time of ~45 min was applied to reach a steady state. Gas lines were heated with electric heating cable between 100 °C and 120 °C to prevent the condensation of water vapor and adsorption of ammonia in the lines. On-line analysis of the products was collected in 3-minute increments by FT-IR spectroscopy (Perkin-Elmer, Frontier TM) in a heated 2-meter gas cell (MARS Series Model #MARS 0.4L/3V-SS, International Crystal Laboratories) set at 120 °C and KBr window (Perkin-Elmer, Frontier TM). The NO and NH_3 conversions were calculated from the concentrations flowing from the inlet to the outlet by using the following equations:

$$\text{NO conversion (\%)} = \frac{[NO]_{Inlet} - [NO]_{Outlet}}{[NO]_{Inlet}} \times 100 \quad (1)$$

$$NH_3 \text{ conversion (\%)} = \frac{[NH_3]_{Inlet} - [NH_3]_{Outlet}}{[NH_3]_{Inlet}} \times 100 \quad (2)$$

RESULTS AND DISCUSSION

1. Characterization of the Catalysts

1-1. Physicochemical Properties

N_2 adsorption-desorption plots showed type I isotherms for H-CHA and series of Cu/CHA catalysts, indicating that all samples contained microporous structure (not shown for brevity). The BET results of different Cu/CHA catalysts are shown in Table 2. The specific surface area of H-CHA sample is 486 m^2/g. Increasing the Cu loading led to a continuous decrease in the BET surface area, while 4.0 wt% Cu/CHA and 5.0 wt% Cu/CHA samples showed similar surface areas, 424 m^2/g and 428 m^2/g, respectively. Compared to H-CHA, 4.0 wt% and 5.0 wt% Cu loading samples' surface areas decreased by ~12%. Increasing the Cu loading further resulted in decreasing the surface area, reaching 415 m^2/g for the sample with the highest Cu loading, 6 wt% Cu-CHA. Although the specific surface areas were decreased with Cu impregnation due to pore blocking, CHA structure was not deformed or collapsed based on the XRD results (explained in the following section).

Table 2. Physical properties of the catalysts

Catalysts	Surface area (m^2/g)
CHA	486
0.5 wt% Cu/CHA	467
1.0 wt% Cu/CHA	465
2.0 wt% Cu/CHA	446
4.0 wt% Cu/CHA	424
5.0 wt% Cu/CHA	428
6.0 wt% Cu/CHA	415

The observed trends are similar to recently reported data from Ndyalkova et al. [22], although the authors used different zeolite framework (BEA), metal species (Fe), and calcination conditions (temperature and time). They suggested impregnation method leads highly dispersed Fe species inside zeolite based on the slightly decreasing, 9%, of surface areas (0.5 wt% Fe-BEA: 567 m^2/g and 4 wt% Fe-BEA: 516 m^2/g). With the series of Cu/FAU and Fe/Cu-SSZ-13 catalysts, Kieger et al. [42] and Zhang et al. [43] also reported decreasing surface areas with increasing Cu and Fe loading due to the microporous channels blocking without destruction of the zeolite structure.

1-2. XRD Analysis

The XRD spectra of fresh Chabazite (CHA) and series of Cu/CHA catalysts are shown in Fig. 1. All the XRD peaks in 2θ= 12.97 ((−110) reflection), 16.17 ((−111) reflection), 20.82 ((−210) reflection), 23.32 ((−121) reflection), 25.27 ((211) reflection), 26.20 ((−220) reflection), and 30.97 ((−131) reflection) showed the typi-

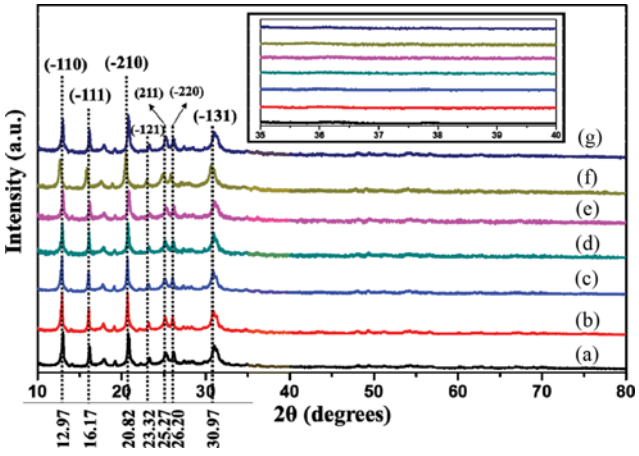

Fig. 1. XRD patterns of (a) CHA, (b) 0.5% Cu/CHA, (c) 1% Cu/CHA, (d) 2% Cu/CHA, (e) 4% Cu/CHA, (f) 5% Cu/CHA, and (g) 6% Cu/CHA samples. Inset: XRD patterns between 35° and 40°.

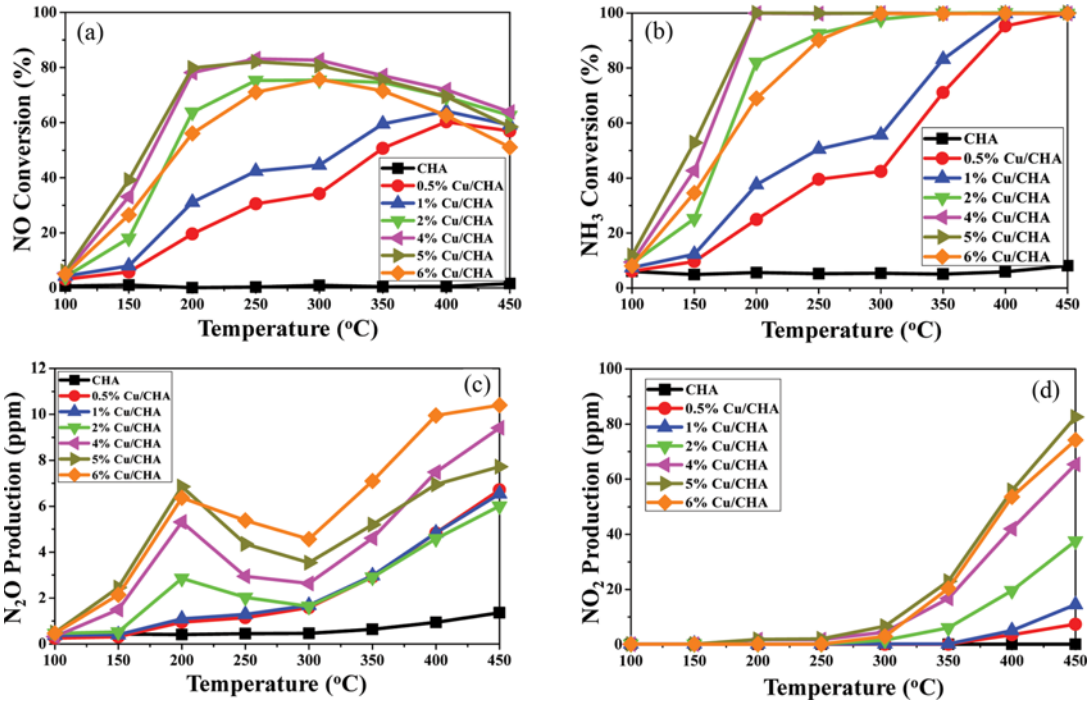

Fig. 2. (a) NO conversion as a function of temperature over Cu-CHA, (b) NH_3 conversion as a function of temperature over Cu-CHA, (c) N_2O formation profiles during NH_3 SCR on Cu-CHA. (d) NO_2 formation profiles during NH_3 SCR on Cu-CHA. Reaction conditions: 50 ml/min (500 ppm) NO, 50 ml/min (500 ppm) NH_3, 10% O_2 balanced with Ar, total flow rate 200 ml/min. ~40 mg sample is used.

cal CHA structure diffraction patterns: a hexagonal unit cell with the space group R3m along with the initial unit cell dimensions of a, b=13.675 Å and c=14.767 Å [44]. This result indicates that the H-CHA sample was highly crystalline and after Cu loading the original zeolite crystalline structure was maintained. Additionally, in Fig. 1, there is no evidence of CuO peaks (36.30° and 38.72°) in the diffraction pattern for any of the Cu loaded samples [16,17]. Recently, Wang et al. [16], reported the XRD patterns of Cu/SAPO-34 synthesized by the solid state ion exchange method and observed CuO phases even at 2.0 wt% Cu loading sample due to the incomplete CuO exchange into the H-SAPO-34. It has been reported that CuO inhibits NH_3-SCR reaction [38]. XRD patterns of fresh and hydrothermally aged zeolites (FAU, CHA, MFI, and BEA) supported Cu samples proved the relationship between CuO and catalytic activity [14,45]. Also, Kwak et al., observed CuO and amorphous zeolite phase for aged Cu-Y, which was related to the complete loss of NH_3-SCR activity. Aforementioned published results suggest that the highly dispersed Cu and prevention of CuO formation during Cu/zeolite synthesis with different catalyst preparation methods will be the first and the most important step for higher catalytic activity. Based on the XRD patterns in Fig. 1, we can conclude that for the Cu/CHA catalysts prepared by incipient wetness method under the conditions employed in this work there are (1) no structural changes in the CHA framework as the Cu content increases and (2) no CuO formation. The XRD patterns are supported by BET results (Table 2), which show a slight decrease in the specific surface area as the Cu loading increases, indicating that Cu ions were well dispersed within the CHA cages without structure deformation [46].

2. Standard NH_3-SCR and NO Oxidation

2-1. Effect of Cu Loading on NH_3-SCR

Standard SCR undergoes a transition in the nature and/or position of active center as a function of temperature; therefore, the effects of Cu loading on the NO_x reduction activity and products' concentrations over Cu/CHA catalysts were examined as a function of reaction temperature between 450 °C to 100 °C, as shown in Fig. 2. Note that we performed NO_x reduction activity test from high (450 °C) to low (100 °C) temperature to avoid any reactant or product gas (after reaction) adsorption into the zeolite pore. Also, H-CHA does not show SCR activity (See Fig. 2(a)). This is a clear indication that Cu sites are the ones responsible for SCR reaction in agreement to previous literature reports on H-SSZ-13, H-ZSM-5, and H-Beta, where the proton form zeolite is not very active for the standard SCR reaction [15,47,48].

Under the present experimental conditions, gradual increase in Cu loading enhanced the NO and NH_3 conversion that reaches maxima while further increase of Cu loading leads to a decrease of the catalytic activity (e.g., 6% Cu/CHA). Optimum Cu loading for the NO conversion was observed with 4 wt% and 5 wt% Cu/CHA catalysts (Fig. 2(a) and 2(b)) that were reaching 80-85% NO conversion at 200 °C to 300 °C. That is four-times higher activity than for 0.5% Cu loading. In Fig. 2(b), although NH_3 conversion results were similar to the NO conversion trends, slightly increased NH_3 conversion indicated that non-selective NH_3 oxidation was also affected by Cu loading and reaction temperature, consequently producing additional NO and a decrease of the SCR activity at high-temperatures. In addition to the Cu loading effects on NO and NH_3 conversion, the reaction temperature at the maximum

NO and NH_3 conversion was shifted to a lower temperature as the copper content increased up to 5 wt%, while 6 wt% Cu/CHA showed lower NO and NH_3 conversion at lower reaction temperatures. These results clearly demonstrate that controlling Cu loading could improve the NO reduction activity and decrease reaction temperature. At >350 °C, most of the samples with higher Cu loading the activity started to decline, and this is in agreement with the result of Ma et al. [37], who observed a decrease in the NO_x conversion at 390 °C on Cu/SAPO-34.

These catalytic trends could be related to the different nature of Cu species for different loadings (supplementary Fig. S1(a) and (b)). Kwak et al. [54] reported that in the ion-exchanged CHA zeolite such as Cu-SSZ-13 two different Cu ions existed in/on Cu-SSZ-13 via H_2-TPR and DRIFTS measurements. They proposed that Cu ions primarily exchanged with protons in the six-membered rings at low Cu loading, while at high Cu loading, Cu is also located in the large cages. A similar positioning was observed with Cu/SAPO-34 [49-51]. Wang et al. [16] showed that as the Cu loading is increased over SAPO-34 the number of the Lewis acid sites monotonically increased while the number of Brønsted acid sites decreased. They also claimed that the Lewis acid sites play a key role in low temperature SCR activity, as we also observed in our result that the NO conversion at low temperature increased due to the increased amount of Cu loading except for 6 wt% Cu/CHA. For the high copper content, the presence of copper oxide species is highly attributed (supplementary Fig. S1(b)). Ayo et al. [52] suggested that Cu first preferentially occupied the ion exchange sites and, once those were saturated, CuO was accumulated. Wang et al. [16] observed different types of Cu structures in the solid state ion exchanged Cu/SAPO-34 samples, such as isolated Cu^{2+} and Cu_xO_y clusters (dimeric or oligomeric Cu species). The SCR reaction is often thought to take place on the isolated Cu^{2+} sites [53]. It was reported that isolated Cu^{2+} increased up to 2.0 wt% Cu loading on SAPO-34 and only slightly increased with higher Cu loading, while the amount of Cu_xO_y clusters continuously increased with increasing Cu loading, and the NH_3 oxidation activity extensively increased with increasing the amount of Cu_xO_y clusters [16]. In our observation we also found that isolated Cu^{2+} sites were responsible for the NH_3-SCR reaction at low temperature, while the Cu_xO_y could catalyze NH_3 oxidation at high temperature. Although dimers were postulated as the active centers for NO decomposition (N_2O and NO_2 formation) [54,55], that is not necessarily attributed to NH_3 -SCR. It can be hypothesized that 6 wt% Cu/CHA contains Cu_xO_y clusters which are related to the lower catalytic activity, which we also noticed from the X-ray photo-electron spectroscopy (XPS) spectra (supplementary Fig. S1(a) and (b)). Even though our XRD results (Fig. 1) do not show the evidence of Cu_xO_y in the 6 wt% Cu/CHA spectrum, it is possible that Cu_xO_y are not crystalline structure or are too small to be detected by XRD. The CuO particles moderately active in nonselective NH_3 oxidation and selectivity of the reaction moved toward N_2O and NO_2 formation [44]. Note that isolated Cu^{2+} ions are intrinsically less active in oxidation reactions than Cu ion dimers and Cu_xO_y clusters. The activity of 6%Cu/CHA (Fig. 2) clearly demonstrates that this is indeed the case. Based on the XRD and XPS, activity results, and literature reviews, we can hypothesize that 5 wt% and 6 wt% samples contain either Cu ion dimers or Cu_xO_y clusters which have undetectable size using the XRD.

Fig. 2(c) and 2(d) display the N_2O and NO_2 concentration profiles, respectively, showing significant differences in product selectivity for different Cu loading samples. Although both 4 wt% and 5 wt% Cu/CHA samples show similar NO and NH_3 conversions, 4 wt% Cu/CHA sample produced lower N_2O and NO_2 concentration (higher N_2 selectivity) compared to 5 wt% Cu/CHA sample in almost the whole reaction temperature ranges. Under the conditions in our study, the highest activity and N_2 selectivity were achieved between 200 °C to 300 °C for the 4% sample. Near 100% selectivity to N_2 during NO reduction reaction was achieved in these temperature regions. Note that N_2O and NO_2 concentrations were <5 ppm up to 350 °C over 4% Cu/CHA catalyst. However, both N_2O and NO_2 concentrations were gradually increased at high temperature, >350 °C, due to the non-selective NH_3 oxidation. The interesting results in Fig. 2(c) are the N_2O production trends with 2-6 wt% Cu/CHA samples through the whole range of temperatures. N_2O production showed a local maximum at 200 °C, then declined and inclined again from 300 °C. Therefore, we can explain N_2O formation as a dual mode mechanism. The low-temperature N_2O formation around 200 °C is a result of NH_3 oxidation by NO that formed NH_4NO_3 surface species and decomposed by the following reaction [56,57]: $NH_4NO_3 \rightarrow N_2O+2H_2O$. Meanwhile, the high temperature N_2O formation was mainly from the oxidation of NH_3 by O_2. Even though N_2 formation by NH_3 oxidation is thermodynamically more favorable ($\Delta G=-327$ kJ/mol) than other products, the pathways leading to N_2O or NO formation are also thermodynamically achievable, $\Delta G=-275$ kJ/mol and $\Delta G=-241$ kJ/mol, respectively [58]. However, N_2O is very stable because the catalytic decomposition of N_2O requires temperatures higher than 450 °C [45]. Ma et al. [37] found that the ammonium nitrate species are more thermally stable on Cu/SAPO-34 compared to Cu/SSZ-13, which leads to less N_2O production during SCR. However, more NO_2 was produced at higher temperature because ammonia oxidation over Cu/SAPO34 is higher compared to Cu/SSZ-13. These phenomena well match our results where we observed higher NO_2 production after 350 °C.

2-2. Water Effect on NH_3-SCR Reaction

The presence of water vapor is inevitable for the application of SCR in diesel engines. Therefore, we further examined the water effect on the catalytic activity and product selectivity in the presence of 2% H_2O. As shown in Fig. 3(a)-(d), the results for NH_3-SCR with presence of 2% H_2O differ, especially N_2O and NO_2 formation, from those obtained in the absence of water.

Water did not inhibit the activity for NO conversion. However, the presence of water slightly increased the SCR activity with increasing the Cu loading and it resulted in a significant improvement of N_2 selectivity at high temperatures. The 4, 5 and 6 wt% Cu/CHA samples show similar activity at temperatures up to 300 °C as measured by NO conversions of ~85%-90%. This is followed by a decline in the activity following the order of 4 wt%<5 wt%< 6 wt% Cu/CHA in the high-temperature regions, 350 °C-450 °C. These results can be interpreted as due to the migration of all Cu species to the large cage to maximize coordination with water. Thus, 4 wt% Cu/CHA maintained the highest activity up to 400°C

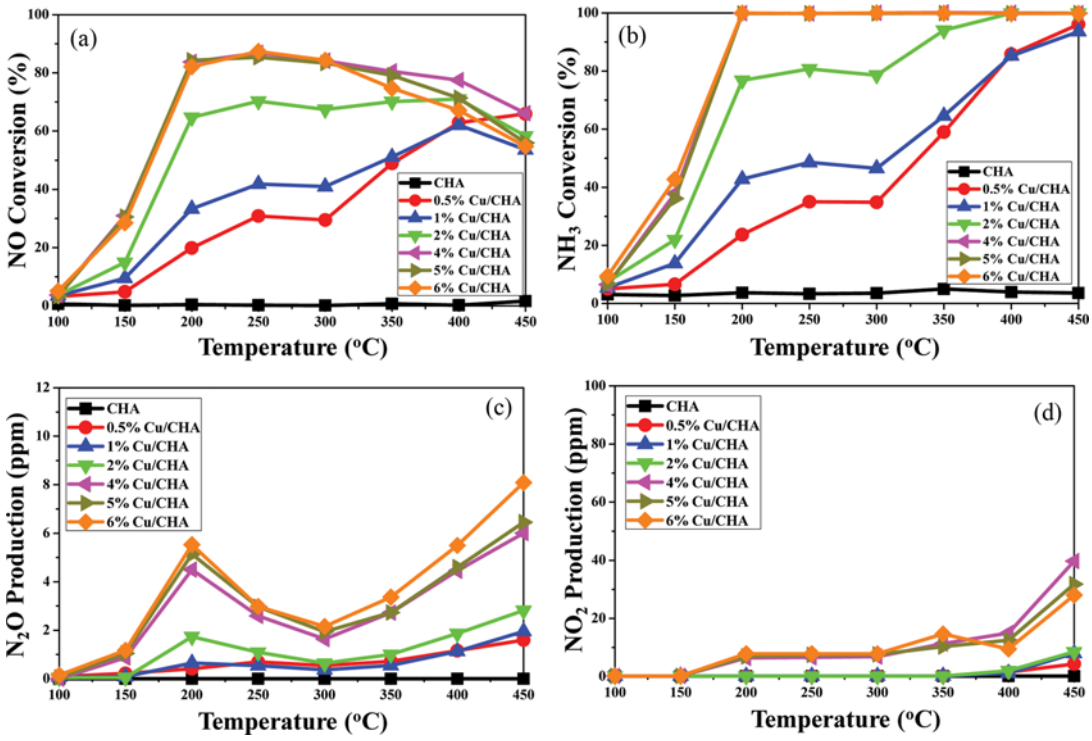

Fig. 3. (a) NO conversion as a function of temperature over Cu-CHA, (b) NH_3 conversion as a function of temperature over Cu-CHA, (c) N_2O formation profiles during NH_3 SCR on Cu-CHA. (d) NO_2 formation profiles during NH_3 SCR on Cu-CHA. Reaction conditions: 50 ml/min (500 ppm) NO, 50 ml/min (500 ppm) NH_3, 10% O_2, 2% H_2O and balanced with Ar, total flow rate 200 ml/min. ~40 mg sample is used.

in the presence of water vapor (Fig. 3(a)), whereas NO conversion started to decline at 300 °C when there was no water, as shown in Fig. 2(a). It was reported that hydrated Cu species are more readily reducible than 'naked' Cu ions [59] because their interaction with zeolite framework weakens, and they have easier access to the reducing agent. Recently, Gao et al. [15] and Kwak et al. [60,61] provided the binding strength and reducibility of Cu^{2+} ions inside the CHA framework by using H_2-TPR and FTIR under hydrated and dehydrated conditions. They concluded that hydrated Cu^{2+} ion monomer (Cu^{2+}-OH) was highly mobile and easily reducible in the presence of moisture due to the lower redox barrier. The enhanced Cu^{2+} mobility and reducibility can decrease the SCR reaction temperature and maintain NO conversion even at higher temperature, in agreement with the results in Fig. 3(a).

Meanwhile, one very interesting phenomenon we observed that the 5 wt% and 6 wt% Cu/CHA samples showed similar activity like 4 wt% at temperatures up to 300 °C. This indicates, at least under hydrated conditions, that the active sites for NH_3-SCR all isolated Cu^{2+} ions are in very similar chemical environments. This observation suggests that with >5 wt% loading samples, the formation of Cu_xO_y clusters on the external surface of SAPO-34 might migrate from isolated Cu^{2+} species formed during the hydration condition. Wang et al. [62] also reported this phenomenon and suggested the generation of more isolated Cu^{2+} ions during aging. And the isolated Cu^{2+} species on Cu-SAPO-34 catalyst was claimed as the active sites for NH_3-SCR reaction in the temperature range 100-200 °C by Li et al. [63,64]. Our observation confirmed that in dehydration condition 5 wt% and higher loading samples have Cu_xO_y clusters presence that generates highly active Cu^{2+} ions during hydration condition. This contributed to the higher number of Cu^{2+} ions that affected the NO_x adsorption and activation on the catalyst surface.

Note that the presence of water in the feed gas results in decreasing N_2O and NO_2 formations. Especially, for the highest reaction temperature at 450 °C, significantly lower N_2O formation was observed, <~8 ppm (Fig. 3(c)). In the case of NO_2, ~50% reduction was observed compared to without water at 450 °C, while NO_2 production slightly increased <300 °C for 4-6 wt% samples. Fig. 3 results confirmed that small amounts of water could inhibit the unselective oxidation of NH_3 and thereby enhance the high-temperature activity. Because, in hydrated condition the Cu_xO_y clusters form isolated Cu^{2+} species whereas Cu_xO_y clusters are responsible for the NH_3 oxidation activity extensively. Furthermore, the presence of water enhanced the activity due to the lower Cu^{2+} reduction barrier as well as the modification of the structure of active sites. Based on these results, we can conclude that the SCR activity and N_2 selectivity increased in the presence of water.

2-3. Effect of Cu Loading on NO Oxidation

NO oxidation has been suggested as the rate-determining step during the "standard" NH_3-SCR reaction [65]. Also, it is well known that the fast SCR [$NO+NO_2+2NH_3 \rightarrow 2N_2+3H_2O$], an equimolar NO/NO_2 ratio, is the most efficient for the conversion of NO_x compared to only NO or NO_2 feed [12]. Thus, the effect of Cu loading on NO oxidation [$2NO+O_2 \rightarrow 2NO_2$] over Cu/CHA was exam-

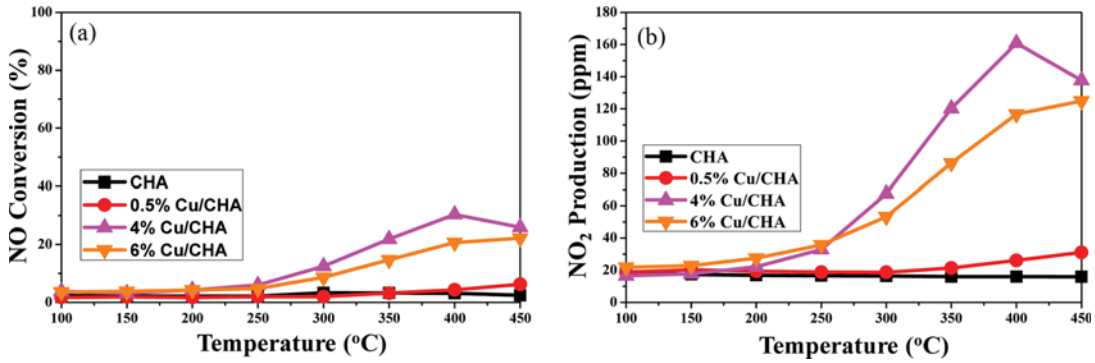

Fig. 4. (a) NO oxidation as a function of temperature over Cu-CHA, (b) NO_2 formation profiles during NO oxidation on Cu-CHA, Reaction conditions: 50 ml/min (500 ppm) NO, 10% O_2, and balanced with Ar, total flow rate 200 ml/min. ~40 mg sample is used.

ined as a function of temperature from 450 °C to 100 °C.

Fig. 4(a) and 4(b) show the NO conversion and NO_2 production for the different Cu containing (0.5 wt%, 4 wt%, and 6 wt% Cu/CHA) catalysts. As shown in Fig. 4(a), the H-CHA sample shows negligible NO oxidation activity. Although NO oxidation over Cu/CHA was also found to be quite low, NO conversion increased with increasing Cu loading and increasing temperatures. Up to 250 °C, NO conversion over 4 wt% and 6 wt% Cu/CHA catalysts is very similar, but 4 wt% Cu/CHA sample shows higher NO conversion at >250 °C. At 400 °C, 4%Cu/CHA sample shows the highest NO conversion, ~32%, which yields ~160 ppm NO_2 production. Further increasing temperature, NO conversion exhibits a slight decrease because the NO/NO_2 thermodynamic equilibrium favors for NO at >400 °C. Also, further increasing of the Cu loading such as for 6%Cu/CHA sample shows lower NO oxidation due to the different types of Cu structures (Supplementary Fig. S1(a) and (b)).

This result shows that the fast SCR reaction does not improve standard NH_3-SCR activity under this experimental condition. This result strongly suggests that NO does not necessarily have to be oxidized to NO_2 for the standard SCR reaction to proceed. Although it has been suggested that NO has to be oxidized to NO_2, which is the rate-determining step of the mechanism [12,66-69], observed results provided that NO is directly activated by Cu species without the NO_2 formation step. Since the 4 wt% Cu/CHA sample shows much higher NO conversion into N_2 during the NH_3-SCR (Fig. 2(a) and 3(a)) at <250 °C than that of 6 wt% Cu/CHA sample, NO oxidation results cannot directly explain how fast SCR involves higher NO conversion (or N_2 selectivity) during the NH_3-SCR reaction. It was reported that NO oxidation cannot be activated over lower Cu loadings (or monomeric Cu ion) on Cu/CHA catalysts, in agreement with our results [13,70,71]. Based on the reported and observed NO oxidation results, it is possible that synthesized 0.5 wt% Cu/CHA sample by impregnated method contains monomeric Cu ion, while 4 wt% and 6 wt% Cu/CHA samples contain dimeric Cu ion. However, NO oxidation activity is still quite low below 300 °C. Therefore, it can be concluded that incipient wetness synthesized Cu/CHA samples are more suitable for reduction than for oxidation of NO.

2-4. Apparent Activation Energies for Reduction and Oxidation of NO

The apparent activation energy for the reduction of NO by NH_3 over impregnated Cu/CHA was calculated using the data obtained at 100 °C-250 °C. Previous studies showed that the SCR reaction is known to be first-order with respect to NO under stoichiometric NH_3 conditions: $r_{NO}=-k[NO]$ [72]. The first-order rate constants

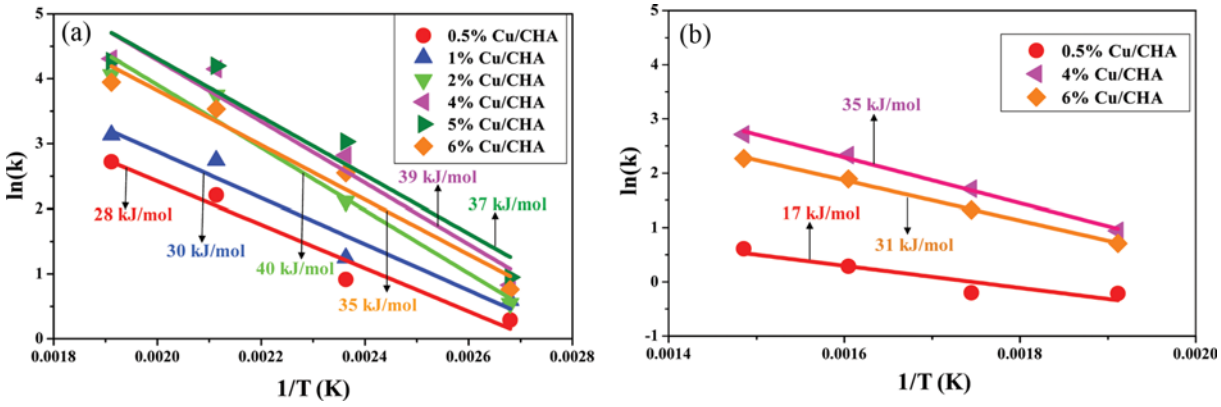

Fig. 5. (a) Arrhenius plot of rate constant (k) for NO reduction versus inverse temperature. Reaction condition: 50 ml/min (500 ppm) NO, 50 ml/min (500 ppm) NH_3, 10% O_2 balanced with Ar, total flow rate 200 ml/min. ~40 mg sample is used. (b) Arrhenius plot of rate constant (k) for NO oxidation versus inverse temperature. Reaction conditions: 50 ml/min (500 ppm) NO, 10% O_2, and balanced with Ar, total flow rate 200 ml/min. ~40 mg sample is used.

were obtained from the conversion of NO as:

$$k = \left(\frac{F_{NO}}{m_{cat} C_{NO}}\right) \ln(1-X) \quad (3)$$

where F_{NO} is the molar feed rate of NO (mol/s), m_{cat} is the catalyst mass, C_{NO} is the NO concentration (mol/cm^3) in the inlet gas and X is the fractional conversion of NO.

Based on the rate constant calculated from Eq. (3), an Arrhenius plot of logarithm of rate constant ln(k) versus inverse temperature was obtained, as shown in Fig. 5(a). The apparent activation energy over the impregnated 0.5 to 6 wt% Cu/CHA catalysts for the NH_3-SCR reaction is 28-40 kJ/mol, which also falls in the range of 29-89 kJ/mol obtained for various zeolites-based SCR catalysts [13,73-76]. Our calculated activation energy is also closely related to the value (41.5±3.7 kJ/mol) over ion-exchanged Cu/SAPO-34 sample, which was prepared by the solid state ion exchanged (SSIE) method by Wang et al. [16]. Interestingly, in our result the more active samples (4% and 5% Cu/CHA) showed the higher E_a and this might be related to the higher number of active sites with those samples that are able to chemisorb more NO_x and lead to obtaining a higher pre-exponential factor, A. This kind of uniqueness is defined as the so-called compensation phenomenon in catalysis [77], which is recalled by Richter et al. [78] and Bond et al. [77] that the rate constant k (Eq. (3)) not only varies with E_a but also with the pre-exponential factor (A), which itself depends on the concentration of active sites.

Additionally, the apparent activation energy for NO oxidation is shown in Fig. 5(b). It was reported that NO oxidation over zeolite-supported metal is also first-order in the reactant NO [59,79,80]. The calculated activation energy (250-400 °C) was 17-35 kJ/mol and this value is in line with previously reported values for other zeolite-based catalysts range of 24-48 kJ/mol [60-62,64]. The activation energy for our impregnated samples displays similar activation energy as ion-exchanged Cu-CHA samples, suggesting identical catalytic centers in both.

CONCLUSIONS

A series of Cu/CHA catalysts were synthesized by incipient wetness method. The physicochemical properties of the catalysts and Cu loading (0.5 wt%-6 wt%) effects were investigated by means of BET, XRD, XPS, standard NH_3-SCR, and NO oxidation reaction. As shown in XRD data, the impregnated Cu did not change the H-CHA structure and indicates that Cu ions were well dispersed within the CHA cages without structure deformation. Catalytic activity and N_2 selectivity during the NH_3-SCR reaction were controlled by both reaction temperature and Cu loading. The NH_3-SCR activity and N_2 selectivity increased with increasing Cu loading up to 4-5 wt%. In the case of >5 wt% Cu loading sample, both NO conversion and N_2 selectivity decreased due to the possible Cu_xO_y cluster formation by XPS observation, even no formation of crystalline Cu_xO_y was observed in the XRD patterns. The highest NO conversion was observed at reaction temperatures 200 °C-300 °C for standard SCR reaction with 4 and 5 wt% Cu/CHA catalysts. The lowest reaction temperature at the highest NO reduction activity shifted with increasing Cu loading up to 4-5 wt%. In the presence of water, NH_3-SCR activity and N_2 selectivity increased due to the enhancement of Cu^{2+} ion mobility and reducibility. NO oxidation activity of Cu/CHA was very low and confirm that Cu/CHA catalysts are poor NO oxidizing catalysts. It appears that the optimum Cu loading via incipient wetness impregnation (IWI) method was 4 wt% for NH_3-SCR reaction. Catalysts prepared by IWI showed similar NH_3-SCR activity, N_2 selectivity, and activation energy to the catalysts prepared by solid state ion-exchange (IE). Thus, the impregnation method is feasible for SCR catalysts synthesis for fundamental research and application of NO conversion during the NH_3-SCR reaction. Finally, the observed results clearly indicate that active Cu sites were affected by experiment conditions, such as Cu loading, dehydration/hydration, and reaction temperature.

ACKNOWLEDGEMENTS

We gratefully acknowledge the financial support from Stony Brook University (SBU) and Brookhaven National Lab (SBU/BNL) 2015 SEED grant (Award #: 37298), as well as Center for Functional Nanomaterials at BNL, which is supported by the U.S. Department of Energy, Office of Basic Energy Sciences, under Contract No. DE-SC0012704 and Advance Energy Centre at SBU for laboratory facilities.

SUPPORTING INFORMATION

Additional information as noted in the text. This information is available via the Internet at http://www.springer.com/chemistry/journal/11814.

REFERENCES

1. M. Chiron, *Stud. Surf. Sci. Catal.*, **30**, 1 (1987).
2. D. L. Mauzerall, B. Sultan, N. Kim and D. F. Bradford, *Atmos. Environ.*, **39**, 2851 (2005).
3. P. J. Crutzen and C. Bruhl, *J. Phys. Chem. A.*, **105**, 1579 (2001).
4. A. R. Ravishankara, *Chem. Rev.*, **103**, 4505 (2003).
5. A. Fritz and V. Pitchon, *Appl. Catal. B Environ.*, **13**, 1 (1997).
6. J. Li, H. Chang, L. Ma, J. Hao and R. T. Yang, *Catal. Today*, **175**, 147 (2011).
7. S. Roy, M. S. Hegde and G. Madras, *Appl. Energy*, **86**, 2283 (2009).
8. F. Gao, J. H. Kwak, J. Szanyi and C. H. F. Peden, *Top. Catal.*, **56**, 1441 (2013).
9. J. Jansson, in Urea-SCR Technology for deNOx After Treatment of Diesel Exhausts, in: I. Nova and E. Tronconi Eds., Springer Science and Business Media, New York (2014).
10. G. Busca, L. Lietti, G. Ramis and F. Berti, *Appl. Catal. B Environ.*, **18**, 1 (1998).
11. R. Q. Long and R. T. Yang, *J. Am. Chem. Soc.*, **121**, 5595 (1999).
12. K. Rahkamaa-Tolonen, T. Maunula, M. Lomma, M. Huuhtanen and R. L. Keiski, *Catal. Today*, **100**, 217 (2005).
13. J. H. Kwak, D. Tran, J. Szanyi, C. H. F. Peden and J. H. Lee, *Catal. Lett.*, **142**, 295 (2012).
14. J. H. Kwak, D. Tran, S. D. Burton, J. Szanyi, J. H. Lee and C. H. F. Peden, *J. Catal.*, **287**, 203 (2012).

15. F. Gao, E. D. Walter, E. M. Karp, J. Luo, R. G. Tonkyn and J. H. Kwak, *J. Catal.*, **300**, 20 (2013).
16. D. Wang, L. Zhang, J. Li, K. Kamasamudram and W. S. Epling, *Catal. Today*, **231**, 64 (2014).
17. D. Wang, L. Zhang, K. Kamasamudram and W. S. Epling, *ACS Catal.*, **3**, 871 (2013).
18. P. G. Blakeman, E. M. Burkholder, H. Y. Chen, J. E. Collier, J. M. Fedeyko and H. Jobson, *Catal. Today*, **231**, 56 (2013).
19. W. Kang, B. Choi and H. Kim, *J. Ind. Eng. Chem.*, **19**, 1406 (2013).
20. J. Kim, A. Jentys, S. M. Maier and J. A. Lercher, *J. Phys. Chem. C.*, **117**, 986 (2013).
21. P. S. Metkar, M. P. Harold and V. Balakotaiah, *Chem. Eng. Sci.*, **87**, 51 (2013).
22. R. Nedyalkova, S. Shwan, M. Skoglundh and L. Olsson, *Appl. Catal. B Environ.*, **138-139**, 373 (2013).
23. S. A. Skarlis, D. Berthout, A. Nicolle, C. Dujardin and P. Granger, *J. Phys. Chem. C.*, **117**, 7154 (2013).
24. U. Deka, I. Lezcano-Gonzalez, B. M. Weckhuysen and A. M. Beale, *ACS Catal.*, **3**, 413 (2013).
25. U. Deka, I. Lezcano-Gonzalez, S. J. Warrender, A. Lorena Picone, P. A. Wright and B. M. Weckhuysen, *Micropor. Mesopor. Mater.*, **166**, 144 (2013).
26. X. Shi, F. Liu, L. Xie, W. Shan and H. He, *Environ. Sci. Technol.*, **47**, 3293 (2013).
27. G. Lv, F. Bin, C. Song, K. Wang and J. Song, *Fuel*, **107**, 217 (2013).
28. C. K. Narula, X. Yang, M. Moses-debusk, D. R. Mullins, S. M. Mahurin and Z. Wu, Final Report Nano Catalysts for Diesel Engine Emission Remediation (2012).
29. W. Xue, P. Burk and S. Boorse, US Patent, 7,601,662 (2009).
30. D. W. Fickel and R. F. Lobo, *J. Phys. Chem. C.*, **114**, 1633 (2010).
31. H. Y. Chen, in Urea-SCR Technology for deNOx After Treatment of Diesel Exhausts, I. Nova and E. Tronconi Eds., Springer Science and Business Media, New York (2014).
32. D. W. Fickel, E. D'Addio, J. A. Lauterbach and R. F. Lobo, *Appl. Catal. B Environ.*, **102**, 441 (2011).
33. Q. Ye, L. Wang and R. T. Yang, *Appl. Catal. A Gen.,* **427-428**, 24 (2012).
34. L. Ma, Y. Cheng, G. Cavataio, R. W. McCabe, L. Fu and J. Li, *Chem. Eng. J.*, **225**, 323 (2013).
35. D. Wang, Y. Jangjou, Y. Liu, M. K. Sharma, J. Luo, J. Li, K. Kamasamudram and W. S. Epling, *Appl. Catal. B Environ.*, **165**, 438 (2015).
36. K. Leistner, O. Mihai, K. Wijayanti, A. Kumar, K. Kamasamudram, N. W. Currier, A. Yezerets and L. Olsson, *Catal. Today*, **258**, 49 (2015).
37. L. Ma, Y. Cheng, G. Cavataio, R. W. McCabe, L. Fu and J. Li, *Appl. Catal. B Environ.*, **156-157**, 428 (2014).
38. C. Petitto and G. Delahay, *Top. Catal.*, **59**, 895 (2016).
39. J. H. Kwak, R. G. Tonkyn, D. H. Kim, J. Szanyi and C. H. F. Peden, *J. Catal.*, **275**, 187 (2010).
40. U. Deka, A. Juhin, E. A. Eilertsen, H. Emerich, M. A. Green and S. T. Korhonen, *J. Phys. Chem. C.*, **116**, 4809 (2012).
41. V. F. Kispersky, A. J. Kropf, F. H. Ribeiro and J. T. Miller, *Phys. Chem. Chem. Phys.*, **14**, 2229 (2012).
42. S. Kieger, G. Delahay, B. Coq and B. Neveu, *J. Catal.*, **183**, 267 (1999).
43. R. Zhang, Y. Li and T. Zhen, *RSC Adv.*, **4**, 52130 (2014).
44. International Zeolite Association. http://www.iza-online.org/ (accessed 19 Feb, 2016).
45. F. Gao, J. H. Kwak, J. Szanyi and C. H. F. Peden, *Top. Catal.*, **56**, 1441 (2013).
46. M. Gomez-Cazalilla, J. M. Merida-Robles, A. Gurbani, E. Rodriguez-Castellon and A. Jimenez-Lopez, *J. Solid State Chem.*, **180**, 1130 (2007).
47. S. Brandenberger, O. Kröcher, A. Tissler and R. Althoff, *Ind. Eng. Chem. Res.*, **50**, 4308 (2011).
48. A. Shishkin, P. A. Carlsson, H. Härelind and M. Skoglundh, *Top. Catal.*, **56**, 567 (2013).
49. L. Wang, J. R. Gaudet, W. Li and D. Weng, *J. Catal.*, **306**, 68 (2013).
50. P. N. R. Vennestrøm, A. Katerinopoulou, R. R. Tiruvalam, A. Kustov, P. G. Moses, P. Concepcion and A. Corma, *ACS Catal.*, **3**, 2158 (2013).
51. M. Zamadics, X. Chen and L. Kevan, *J. Phys. Chem.*, **96**, 5488 (1992).
52. B. Pereda-Ayo, U. De La Torre, M. J. Illán-Gómez, A. Bueno-López and J. R. González-Velasco, *Appl. Catal. B Environ.*, **147**, 420 (2014).
53. J. Xue, X. Wang, G. Qi, J. Wang, M. Shen and W. Li, *J. Catal.*, **297**, 56 (2013).
54. S. Kieger, G. Delahay, B. Coq and B. Neveu, *J. Catal.,* **183**, 267 (1999).
55. G. Delahay, B. Coq, S. Kieger and B. Neveu, *Catal. Today*, **54**, 431 (1999).
56. K. Kamasamudram, C. Henry, N. Currier and A. Yezerets, *SAE Int. J. Engines.*, **5**, 688 (2012).
57. G. J. Bartley and C. Sharp, *SAE Int. J. Engines.*, **5**, 683 (2012).
58. K. Kamasamudram, A. Yezerets, X. Chen, N. Currier, M. Castagnola and H.-Y. Chen, *SAE Int. J. Engines.*, **4**, 1810 (2011).
59. F. Gao, N. M. Washton, Y. Wang, M. Kollar, J. Szanyi and C. H. F. Peden, *J. Catal.*, **331**, 25 (2015).
60. J. Hun Kwak, H. Zhu, J. H. Lee, C. H. F. Peden and J. Szanyi, *Chem. Commun.*, **48**, 4758 (2012).
61. J. H. Kwak, T. Varga, C. H. F. Peden, F. Gao, J. C. Hanson and J. Szanyi, *J. Catal.*, **314**, 83 (2014).
62. J. Wang, T. Yu, X. Wang, G. Qi, J. Xue, M. Shen and W. Li, *Appl. Catal. B Environ.*, **127**, 137 (2012).
63. L. Wang, W. Li, G. Qi and D. Weng, *J. Catal.*, **289**, 21 (2012).
64. J. Xue, X. Wang, G. Qi, J. Wang, M. Shen and W. Li, *J. Catal.*, **297**, 56 (2013).
65. S. Brandenberger, O. Kröcher, A. Tissler and R. Althoff, *Cat. Rev.-Sci. Eng.*, **50**(4), 492 (2008).
66. M. Devadas, O. Krocher, M. Elsener, A. Wokaun, N. Soger and M. Pfeifer, *Appl. Catal. B Environ.*, **67**, 187 (2006).
67. G. Delahay, D. Valade, A. Guzmanvargas and B. Coq, *Appl. Catal. B Environ.*, **55**, 149 (2005).
68. H. Y. Huang, R. Q. Long and R. T. Yang, *Appl. Catal. A Gen.*, **235**, 241 (2002).
69. R. Q. Long and R. T. Yang, *J. Catal.*, 207, 224 (2002).
70. F. Gao, E. D. Walter, M. Kollar, Y. Wang, J. Szanyi and C. H. F. Peden, *J. Catal.*, **319**, 1 (2014).
71. A. A. Verma, S. A. Bates, T. Anggara, C. Paolucci, A. A. Parekh and K. Kamasamudram, *J. Catal.*, **312**, 179 (2014).
72. R. Q. Long and R. T. Yang, *J. Catal.*, **196**, 73 (2000).

73. J. S. McEwen, T. Anggara, W. F. Schneider, V. F. Kispersky, J. T. Miller and W. N. Delgass, *Catal. Today*, **184**, 129 (2012).
74. H. Sjövall, R. J. Blint and L. Olsson, *Appl. Catal. B Environ*., **92**, 138 (2009).
75. T. J. Wang, S. W. Baek, H. J. Kwon, Y. J. Kim, I. S. Nam and M. S. Cha, *Ind. Eng. Chem. Res*., **50**, 2850 (2011).
76. A. Pant and S. J. Schmieg, *Ind. Eng. Chem. Res.*, **50**, 5490 (2011).
77. G. C. Bond, M. A. Keane, H. Kral and J. A. Lercher, *Catal. Rev. Sci. Eng*., **42**, 323 (2000).
78. M. Richter, U. Bentrup, R. Eckelt, M. Schneider, M.-M. Polh and R. Fricke, *Appl. Catal. B: Environ*., **51**, 261 (2004).
79. M. Colombo, I. Nova and E. Tronconi, *Catal. Today*, **151**, 223 (2010).
80. P. S. Metkar, N. Salazar, R. Muncrief, V. Balakotaiah and M. P. Harold, *Appl. Catal. B Environ*., **104**, 110 (2011).
81. A. M. Beale, F. Gao, I. Lezcano-Gonzalez, C. H. F. Peden and J. Szanyi, *Chem. Soc. Rev*., **44**, 7371 (2015).
82. M. Schreier, S. Teren, L. Belcher, J. R. Regalbuto and J. T. Miller, *Nanotechnology*, **16**, S582 (2005).
83. Y. Zuo, L. Han, W. Bao, L. Chang and J. Wang and C. Xuebao, *Chinese J. Catal*., **34**, 1112 (2013).
84. Y. Li, J. Deng, W. Song, J. Liu, Z. Zhao, M. Gao and Y. Wei, *J. Phys. Chem. C.* **120**, 14669 (2016).

Supporting Information

Effects of copper loading on NH_3-SCR and NO oxidation over Cu impregnated CHA zeolite

Nusnin Akter*, Xianyin Chen, John Parise**, Jorge Anibal Boscoboinik*,***, and Taejin Kim*,†**

*Materials Science and Chemical Engineering Department, Stony Brook University, Stony Brook, NY 11794, U.S.A.
**Geosciences Department, Stony Brook University, Stony Brook, NY 11794, U.S.A.
***Center for Functional Laboratory, Brookhaven National Laboratory, Upton, NY 11973, U.S.A.
(*Received 1 July 2017 • accepted 25 September 2017*)

To study the state of Cu species on the surface we investigate the binding energy of the Cu 2p transition peaks of the Cu/CHA catalysts. Fig. S1(a) shows XPS spectra of Cu 2p of 2, 4, and 6% Cu/CHA samples. As can be seen, two peaks were observed at ~935 eV and ~955 eV, which are corresponding to Cu $2p_{3/2}$ and Cu $2p_{1/2}$, respectively. In addition to these peaks, shake-up satellite peak was also observed which is corresponding Cu^{2+}. However, Cu^0 species was not observed which appears at higher binding energy than Cu $2p_{3/2}$. Moreover, in many literatures the other satellite shakeup peak around 963 eV (which is higher binding energy than Cu $2p_{1/2}$) was reported [69,83,84]. However this 963 eV satellite peak is missing in our data because there is an overlap with the ascending KLL Auger line of O_2. However, these satellites can be assigned to the charge transfer between the transition metal 3d and surrounding ligand oxygen 2p orbitals. In Fig. S1(b), for three samples we closely look into the main Cu $2p_{3/2}$ peak which is deconvoluted into three contributions around 932.2, 934.4, and 936 eV. This kind of deconvolution is also reported in Li et al. for the Cu-SAPO-18 catalysts prepared by incipient wetness method [84]. The peak at 932.2 eV is assigned to Cu(I) species including isolated Cu^+ ions and Cu_2O. This peak is more prominent for the 4% and 6% Cu/CHA. The peak at 936 eV corresponds to the Cu^{2+} ions coordinating to framework oxygen atoms of CHA zeolite, and this peak is present for all the samples. The peak at 934.4 eV is assigned to CuO species on the zeolite and this is more intense for the 6% Cu/CHA sample than others while the peak corresponds to the Cu^{2+} ions (936 eV) remains the same for all samples. Therefore, we can state that this excess amount of CuO on 6% Cu/CHA is responsible for the lower SCR activity as well as pore blocking (Table 2). While in presence of water the SCR activity is increased specially in low temperature almost similar like 4% Cu/CHA. This result indicates that copper species undergo significant changes during hydrothermal treatment. It can be explained that agglomerated copper oxides on the surface migrated inside the pores during hydrothermal treatment and formed isolated Cu^{2+} species (Lewis acid sites) that decrement low temperature SCR activity, where CuO do not show acidic properties [16,49].

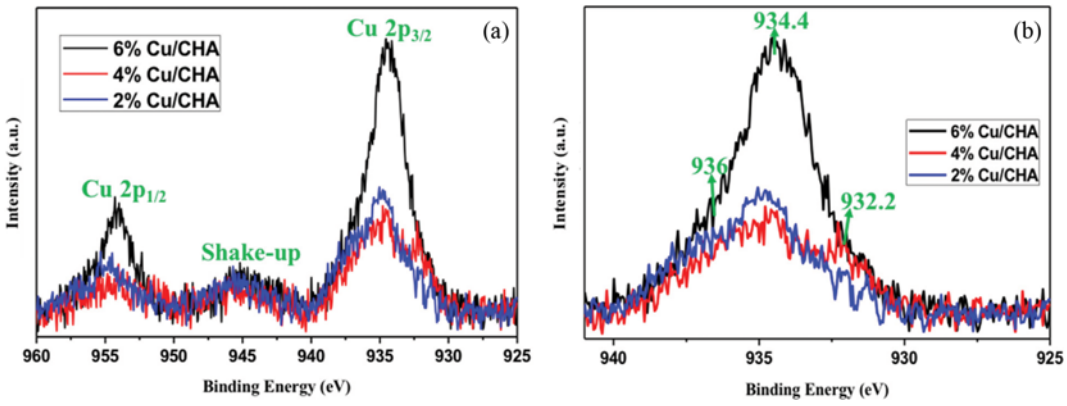

Fig. S1. Cu 2p X-ray photo-electron spectroscopy (XPS) spectra of 2, 4, and 6% Cu/CHA samples (a) Full scale of 925-960 eV (b) magnified region of 925-940 eV.